Journal of Applied Electrochemistry **33**: 577–587, 2003.

Electrodiffusion detection of the near-wall flow reversal in liquid films at the regime of solitary waves

J. TIHON*, V. TOVCHIGRECHKO, V. SOBOLÍK and O. WEIN
Institute of Chemical Process Fundamentals, Academy of Sciences of the Czech Republic, Rozvojová 135, 16502 Prague 6, Czech Republic
*(*author for correspondence, e-mail: tihon@icpf.cas.cz)*

Received 27 September 2002; accepted in revised form 11 March 2003

Key words: electrodiffusion technique, flow reversal, probe response, wavy film flow

Abstract

The liquid film flow down an oscillating plate was used as a suitable flow configuration to study the dynamic behaviour of electrodiffusion friction probes at large fluctuations. The two-segment probe was flush mounted into the plate wall to measure the fluctuating wall shear rate. The hydrodynamics of the experiment made it possible to adjust both the steady and oscillatory component of the wall shear rate through the operation parameters (flow rate, plate inclination, amplitude and frequency of wall oscillations). The approximate model of the probe dynamic response based on the similarity of concentration profiles at the probe surface was verified. This simple model proved to be able to calculate the instantaneous wall shear rate from the measured current signal even at large flow fluctuations. The analysis of the probe dynamic behaviour under reversing flow conditions provided a new method of the detection of short-time flow reversal. Finally, this method was successfully applied to confirm the existence of a small backflow region located in front of the large solitary waves, which were excited on the surface of a liquid film flowing down an inclined stationary plate.

List of symbols

a amplitude of the plate oscillations (m)
A_{ED} amplitude attenuation of the electrodiffusion signal (Equation 9)
A_{HD} amplitude attenuation of the wall shear rate signal (Equation 13)
A_R ratio of the signal amplitudes $= (\tilde{I}_R/\bar{I}_R)/(\tilde{\dot{\gamma}}/\bar{\dot{\gamma}})$
c wave velocity (m s^{-1})
c_0 concentration of the active ions (kmol m^{-3})
D diffusion coefficient (m^2 s^{-1})
D_s diffusion coefficient determined from the measured value of k_s (Equation 5) (m^2 s^{-1})
D_t diffusion coefficient determined from the measured value of k_t (Equation 6) (m^2 s^{-1})
f frequency (Hz)
f_P frequency of the flow rate pulsations (Hz)
F faradaic constant (9.648×10^7 C $kmol^{-1}$)
g gravitational acceleration (9.81 m s^{-2})
g_i thickness of the insulating gap (m)
h film thickness (m)
H^*_{ED} transfer function of the probe current response to the wall shear rate modulation
H_0 quasisteady response of the electrodiffusion probe $= \bar{I}/(3\bar{\dot{\gamma}})$ (A s)
I probe current (A)
I_1 current from the front probe segment (A)
I_2 current from the rear probe segment (A)
I_R current ratio $= I_2/I_1$
l length of the probe strip in the mean flow direction (m)
k_s steady flow calibration constant of the probe (A $s^{1/3}$)
k_t dynamic calibration constant of the probe (A $s^{1/2}$)
Q volumetric flow rate per unit span of the plate (m^2 s^{-1})
Re Reynolds number $= Q/v$

St Stokes number $= h(\omega/\nu)^{1/2}$
t time (s)
t_0 characteristic time of the electrodiffusion probe (Equation 7) (s)
w width of the probe strip (m)
x distance of the oscillating plate from the displacement transducer (m)
X axial distance from the liquid distributor (m)
z number of electrons involved in the redox reaction

Greek symbols
α inclination angle of the plate (deg)
$\dot{\gamma}$ wall shear rate (s^{-1})
Φ_{ED} phase shift of the electrodiffusion signal in respect to the wall shear rate (Equation 10)
Φ_{HD} phase shift of the wall shear rate in respect to the wall oscillations (Equation 11)
λ wave length (m)
ν kinematic viscosity ($m^2\ s^{-1}$)
ρ density ($kg\ m^{-3}$)
ω angular frequency $= 2\pi f$ ($rad\ s^{-1}$)
Ω dimensionless frequency $= \omega t_0$
Ω_1 dimensionless frequency calculated for the front probe segment $= \omega(k_t/\bar{I}_1)^2$

Superscripts
– time-average value
$\sim$ amplitude of the fluctuating signal

1. Introduction

The electrodiffusion technique using probes flush mounted into a wall is often used to measure local values of the wall shear rate [1, 2]. The probe active surface works as a small electrode where a fast electrochemical reaction takes place. The measured limiting current is controlled by convective diffusion and the well-known Léveque formula can be applied to determine the wall shear rate. The main advantage of this technique is that the wall probes provide information about the flow in the near wall region without any disturbances imposed on the studied velocity field. On the other hand, to interpret the results of measurements performed under unsteady flow condition, the dynamic response of the concentration boundary layer near the probe surface to the flow fluctuations has to be considered.

If relatively small fluctuations of the wall shear rate are assumed, the equation of unsteady mass transport can be solved with the aim of obtaining the transfer function of the probe response [3–5]. This prediction was confirmed by experiments performed in the modulated flow configuration of a rotating disc [6]. The transfer function is used to calculate the amplitude attenuation and the phase shift of the measured current signal in respect to the imposed wall shear rate variation of a given frequency. It also makes it possible to correct the power spectra obtained from the measurements of near-wall turbulence.

The probe dynamic response in large amplitude unsteady flows has been much less investigated [7, 8]. It was shown that the distortion of the measured signal in respect to the quasi-steady one becomes stronger as the amplitude of imposed fluctuations increases. The amplitude attenuation and the phase shift are especially significant in the region around the wall shear rate minimum where convection is small and the probe inertia becomes significant.

The inverse problem of calculating the instantaneous wall shear rate from the measured current signal has to be solved to acquire the near-wall flow variation in a whole time domain. The numerical approach to the inverse problem solution [9] suggests the procedure that is too complicated from a practical point of view. An approximate model of the wall probe dynamics [10, 11] seems to be more useful for experimental data treatment. This simple model is based on the assumption of similarity in the concentration fields established near the probe surface under steady and unsteady flow conditions. It is capable to provide a satisfactory dynamic correction of the measured signal even for quite large amplitudes of the flow modulation [12].

The single wall probe is applicable only under nonreversing flow conditions. If flow reversal occurs in the near-wall flow region and additional information about the flow direction is needed, the two-segment probe [13, 14] is usually applied. This 'sandwich probe' consists of two active segments separated in the mean flow direction by a thin insulating gap. If the studied reversing flow exhibits a steady recirculation zone, as in backward-facing step flow [15] and in flow around a cylinder [16], or if local changes of the flow direction are relatively slow, as in the liquid film flow driven by air blowing [17], the experimental detection of the flow

reversal is easy. In these cases the direction of the flow is detected by a simple comparison of the magnitudes of current signals flowing through the front and rear probe segment. The correct interpretation of signals measured by a two-segment probe under highly unsteady flow conditions is more complicated due to the necessity to consider different dynamic behaviour of individual segments of the probe.

Wavy film flow down an inclined plane is a typical representative of unsteady flows. The spatio-temporal evolution of waves on the film surface is a complex process and the different kinds of waves can be observed. Small-amplitude waves appearing at the wave inception grow rapidly and develop downstream into the large nonlinear patterns of finite-amplitude, solitary or three-dimensional waves [18]. The large solitary waves (sometimes called 'rolling waves') are separated by wide regions of the thin liquid film and have a typical shape characterized by a steep front and a gradual tail. Small capillary waves are usually pushed in front of these solitary waves. This region is not easy accessible for the experimental investigation, because rapid flow changes observed there take place inside the thin liquid film. The recent numerical simulation of wavy film flow [19] has suggested that there is possibly a small backflow region in front of the large solitary waves. It has been a challenge for us to confirm or reject such a surprising finding by the relevant electrodiffusion experiments.

The main purpose of this paper is to suggest a new method of performing dynamic calibrations of two-strip electrodiffusion probes and subsequent treatment of data obtained by such a probe under highly unsteady flow conditions. The results of our calibration experiments carried out under oscillating film flow conditions show that the two-strip probe is able to detect the near-wall flow reversal even if its duration is relatively short. The results of wavy film flow investigation then demonstrate that this probe can provide valuable information about the near-wall flow. In this test case, the wall shear rate measurements confirm the existence of a small backflow region located just in front of a large solitary wave travelling down the liquid film.

2. Dynamic response of the electrodiffusion friction probes

Only if the flow fluctuations are slow enough, can the limiting diffusion current $I(t)$ be directly related to the instantaneous value of the wall shear rate $\dot{\gamma}(t)$. For a single strip probe this quasisteady relation can be expressed in the following well-known form:

$$I(t) = 0.807\, zFc_0 wl^{2/3} D^{2/3} \dot{\gamma}^{1/3}(t) \tag{1}$$

where z, F, l, w, c_0 and D have the meanings described at the outset. For proper use of electrodiffusion probes under unsteady flow conditions, it is necessary to consider their dynamic response. The approximate model [11] suggested for description of the probe dynamic behaviour is represented by the simple formula

$$\dot{\gamma} = k_s^{-3}\left(I^3 + 2k_t^2 \frac{\mathrm{d}I}{\mathrm{d}t}\right) \tag{2}$$

This semi-empirical differential equation contains two constants, easily accessible from the steady flow calibrations. The first constant k_s corresponds to the steady state solution

$$I = k_s \dot{\gamma}^{1/3} \tag{3}$$

and the second one k_t can be determined from the known solution of the unsteady diffusion at the beginning of the transient process after the probe polarization switch-on

$$I = k_t t^{-1/2} \tag{4}$$

If the exact shape of a probe and the diffusivity of ions involved in the electrode reaction are known, both the constants can also be calculated from the theoretical relationships. For a single strip probe

$$k_s = 0.807\, zFc_0 wl^{2/3} D^{2/3} \tag{5}$$

and

$$k_t = zFc_0 wl\sqrt{D/\pi} \tag{6}$$

To estimate the single probe inertia at given flow conditions characterized by the value of $\bar{\dot{\gamma}}$, the characteristic time parameter t_0 can be introduced as

$$t_0 = (k_t/\bar{I})^2 = (k_t/k_s)^2 \bar{\dot{\gamma}}^{-2/3} \tag{7}$$

This parameter is determined as the time coordinate of the intersection of both the asymptotes (Equations 3 and 4) of the transient current response after the probe polarization switch-on. The dependence of this characteristic time on the actual flow conditions represented by the mean value of wall shear rate is an important consequence of nonlinear dynamic behaviour of the electrodiffusion probes.

We can also consider the electrodiffusion probe as a dynamic system, where the input is a harmonically superposed wall shear rate and the output is a current response of the probe. Following the linear theory of small-amplitude fluctuations, the transfer function of the probe current response to the wall shear rate modulation, $H^*_{ED}(\Omega)$, can be obtained. This complex function of the frequency can be represented by the pair of real-value functions: the amplitude attenuation $A_{ED}(\Omega)$ and phase shift $\Phi_{ED}(\Omega)$. The approximate model (Equation 2) provides the differential equation that leads to the frequency response function

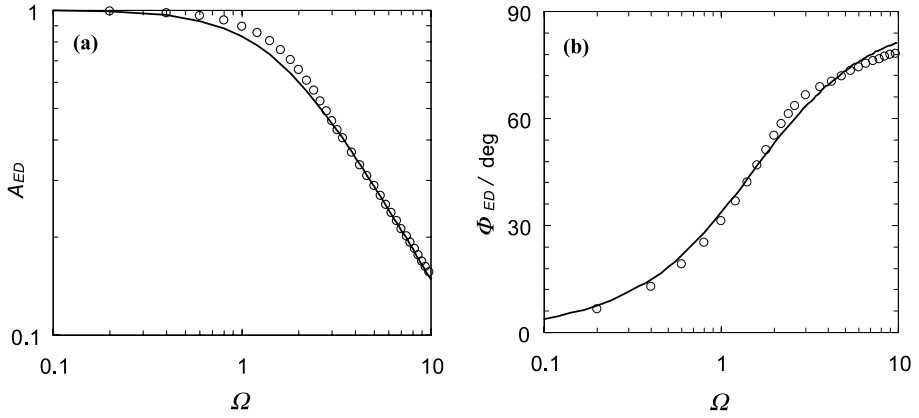

Fig. 1. Frequency response of a single electrodiffusion probe: (a) amplitude attenuation, (b) phase shift. Approximate solution (Equations 9 and 10, *lines*) is compared with the exact results for a strip probe (*symbols*).

$$H^*_{\mathrm{ED}} = H_0 A_{\mathrm{ED}} \exp(-\mathrm{i}\Phi_{\mathrm{ED}}) = \frac{\bar{I}/\bar{\dot{\gamma}}}{3 + \mathrm{i}2\Omega} \tag{8}$$

where the dimensionless frequency $\Omega = \omega t_0$ is based on the probe characteristic time t_0 and $H_0 = \bar{I}/(3\bar{\dot{\gamma}})$ is a quasisteady impedance valid for $\Omega \to 0$. It is clearly seen in Figure 1 that the simple formulas for the amplitude attenuation

$$A_{\mathrm{ED}} = \frac{1}{\sqrt{1 + \frac{4}{9}\Omega^2}} \tag{9}$$

and for the phase shift

$$\Phi_{\mathrm{ED}} = \arctan\left(\frac{2}{3}\Omega\right) \tag{10}$$

predicted by the approximate model agree well with the exact results obtained for a single strip probe from the numerical solution [5].

Let us consider now the probe with two parallel strips of the same length separated in the flow direction by a thin insulating gap. Assuming that the insulating gap between the segments is infinitesimally thin, the dynamic response of the rear (downstream) segment can be determined as the difference between the current responses of 'the overall probe' (strip of the length of $2l$) and the front (upstream) segment (strip of the length of l). Consequently the numerical results [5] obtained for a single probe can be also used to estimate dynamic behaviour of the individual segments of the two-strip probe. The dynamic responses calculated for the overall probe and for the individual probe segments are presented in Figure 2. The dynamic response of the front segment is qualitatively same as that of the overall probe and both the responses would be identical if comparison is based on Ω (same dimensionless frequency) instead of Ω_1 (same flow conditions) used in Figure 2. Due to the absence of sensitive leading edge, the response of rear segment is similar to the local response observed at a certain distance from the leading edge [4]. This is reason why both the segments exhibit different asymptotic behaviour at high frequencies: the amplitude attenuation is proportional either to Ω_1^{-1} (front segment, single probe asymptote) or to $\Omega_1^{-3/2}$ (rear segment, local asymptote) and the corresponding asymptotic phase shift is $\Phi_{\mathrm{ED}} = 90°$ or 135°, respectively.

The two-strip probe should evidently provide more complex information about the studied flow. However, the question is how can this information be interpreted.

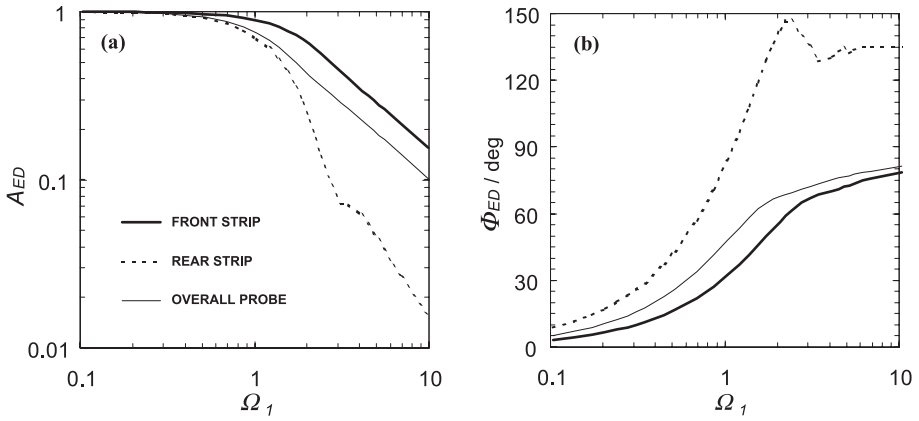

Fig. 2. Frequency response of a two-strip probe: (a) amplitude attenuation, (b) phase shift. Numerically calculated responses of the front (*thick line*) and rear (*dashed line*) strip are compared with that of the overall probe (*thin line*).

A promising approach is to analyse the dynamic response of certain combinations of the current signals provided by the probe segments. It was demonstrated by Py [20] that this approach could improve the frequency response of the probe. Below, in the experimental part of this work, our attention will be focused on dynamic behaviour of the current ratio signal, $I_R = I_2/I_1$. It will be shown how this signal should be treated to obtain information on the amplitude of large wall shear rate fluctuations.

3. Description of the experiments

3.1. *Model fluids and electrochemical system*

Water, two aqueous solutions of glycerine (30% and 50% by weight), and two aqueous solutions of polyalkylene glycol EmkaroxHV40 (6% and 10% by weight) were chosen as the model liquids. A suitable electrochemical system was provided by the addition of 0.025 M equimolar potassium ferro/ferricyanide and 0.05 M potassium sulfate. The resulting solutions differed significantly in the value of diffusivity of ferricyanide ions (see Table 1 below). The versatile two-segment probe was manufactured from two platinum foils that were glued into a stainless steel tube. The front profiles of platinum foils acted as two parallel strip cathodes and the tube served as a counterelectrode. Both probe strip segments had the same size ($l = 0.1$ mm and $w = 1$ mm). The strip with longer side w was always oriented perpendicularly to the flow direction. The thickness of the insulating gap g_i between the two strip segments was about 0.01 mm. A polarization voltage of −0.8 V was applied to assure that the probe was working under limiting diffusion current conditions. A home built electrodiffusion analyser set the polarization voltage to the probe, converted currents flowing through the individual segments into voltages and amplified the resulting signals. A PC provided with an A/D and D/A card controlled this analyser.

3.2. *Experimental outline*

Three types of experiments were performed in successive steps:

(a) Probe calibration under steady flow conditions of the viscometric flow between two coaxial cylinders (see Sections 3.3 and 4.1):
   (i) dependence of the limiting diffusion current on the wall shear rate provides k_s,
   (ii) transient current response after switch on of the probe potential provides k_t.
(b) Probe calibration under pulsatile flow conditions of the non-wavy film flow down an oscillating plate (see Sections 3.4 and 4.2):
   (i) verification of the approximate model of the probe dynamic behaviour,
   (ii) experimental determination of the frequency response function for the two-strip probe,
   (iii) analysis of the current ratio signal I_R aimed to the detection of unsteady flow reversal.
(c) Wall shear rate measurements in the wavy film flow artificially excited by the inlet flow rate pulsations (see Sections 3.5 and 4.3).

3.3. *Calibrations under steady flow conditions*

The probe was calibrated in a special device involving two coaxial cylinders (Figure 3). It was inserted into the outer cylinder wall and the solution filled the gap between the cylinders. The inner cylinder rotation provided laminar Couette flow conditions in the device. The rotation speed was changed to provide wall shear rates ranging from 20 s^{-1} to 400 s^{-1}. The corresponding limiting diffusion currents flowing through the probe segments were measured to determine the calibration constants k_s and k_t for each model liquid.

3.4. *Calibrations done under fluctuating flow conditions*

The probe calibrations under fluctuating flow conditions were performed in the experimental set-up shown in Figure 4. The liquid film was produced on a smooth stainless steel plate (0.8 m in length and 0.15 m in

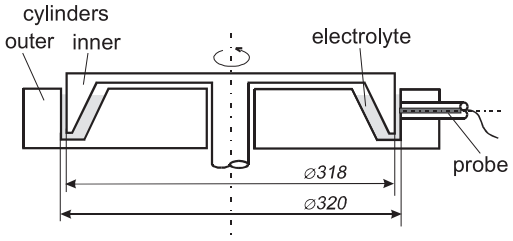

Fig. 3. Experimental set-up for steady flow calibrations of the wall probes.

Table 1. Viscosity, density, diffusivity, and calibration constants of the model liquids

Liquid	Water	Emkarox 6%	Emkarox 10%	Glycerin 30%	Glycerin 50%
$\nu \times 10^6/m^2\ s^{-1}$	1.0	6.1	12.4	2.5	6.0
$\rho/kg\ m^{-3}$	1000	1032	1035	1076	1136
$k_t/\mu A\ s^{1/2}$	4.35	3.41	3.10	2.50	1.72
$k_s/\mu A\ s^{1/3}$	4.06	2.85	2.60	1.82	1.12
$D_t/m^2\ s^{-1}$	7.96×10^{-10}	4.89×10^{-10}	4.04×10^{-10}	2.63×10^{-10}	1.24×10^{-10}
$D_s/m^2\ s^{-1}$	8.28×10^{-10}	4.62×10^{-10}	4.25×10^{-10}	2.49×10^{-10}	1.20×10^{-10}

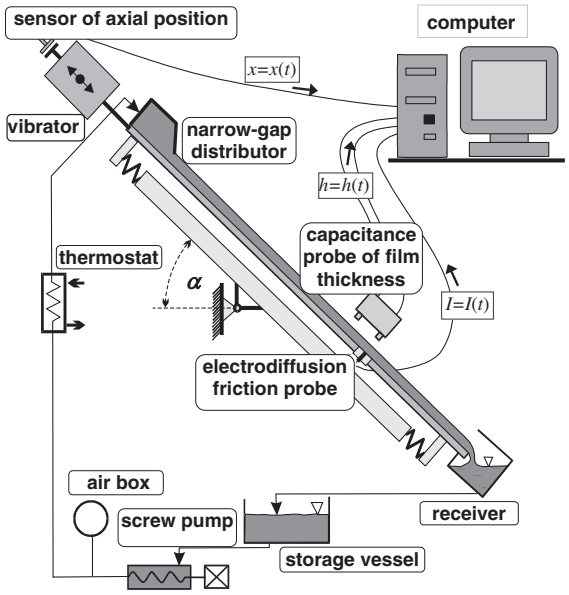

Fig. 4. Experimental set-up for dynamic calibrations of the wall probes.

width). The plate slope could be changed from the vertical to the horizontal position. An electromagnetic vibrator was used to impose oscillations parallel to the film flow direction on the plate. The frequency of these oscillations was changed in the range of f from 0 to 50 Hz and their amplitude was adjusted up to the maximal value of $a = 3$ mm. Three types of signal were measured: the film thickness $h(t)$ (by a capacitance probe [11]), the limiting diffusion current $I(t)$ (by an electrodiffusion probe), and the axial position of the plate $x(t)$ (by a displacement transducer).

If the laminar, non-wavy liquid film is flowing down an oscillating wall, the time course of wall shear rate can be expressed as

$$\dot{\gamma}(t) = \bar{\dot{\gamma}} + \tilde{\dot{\gamma}} \sin(\omega t + \Phi_{HD}) \tag{11}$$

The time-average component of wall shear rate $\bar{\dot{\gamma}}$ is dependent on three hydrodynamic parameters (kinematic viscosity v, liquid film thickness h, and plate inclination angle α):

$$\bar{\dot{\gamma}} = g \sin\alpha \frac{h}{v} \tag{12}$$

The amplitude of wall shear rate fluctuations $\tilde{\dot{\gamma}}$ is controlled by two parameters of the plate oscillations (their angular frequency ω and amplitude a):

$$\tilde{\dot{\gamma}} = A_{HD} a \omega^2 \frac{h}{v} \tag{13}$$

The hydrodynamic response of the fluctuating wall shear rate to the wall oscillation motion is represented by two functions of the Stokes number ($St = h(\omega/v)^{1/2}$): the hydrodynamic phase shift $\Phi_{HD}(St)$ and amplitude attenuation $A_{HD}(St)$. The actual values of these functions, which range between $\Phi_{HD} = 90°$, $A_{HD} = 1$ (low-frequency limit, for $St \to 0$) and $\Phi_{HD} = 135°$, $A_{HD} = 0$ (high-frequency limit, for $St \to \infty$), can be found together with a detailed analysis of the oscillating film flow in [21].

3.5. *Wavy film flow experiments*

The experimental investigation of the wavy film flow was carried out in an experimental set-up similar to that shown in Figure 4. The liquid film flowed down a long stationary plate (2 m in length and 0.22 m in width). This stainless steel plate was fixed at a constant inclination angle $\alpha = 6.5°$. A piston mounted into the air chamber produced periodical pulsations of the flow rate with a small amplitude (up to 10% of the mean flow rate) and low frequency (from 0.5 to 2.5 Hz). These low-frequency pulsations excited regular solitary waves on the liquid film surface. The two-strip electrodiffusion probe was mounted into the wall to detect the wall shear rate under large solitary waves. The capacitance probe, installed at the same distance from the liquid distributor ($X = 1.5$ m) as the electrodiffusion one, simultaneously measured the instantaneous film thickness. These measurements were carried out with water as the model liquid.

4. Results and discussion

4.1. *Steady flow calibrations of the two-segment electrodiffusion probe*

These measurements provided the probe calibration constants for the different model liquids. The pairs of constants (k_s and k_t), obtained for the front probe segment, are presented, together with the physical properties of the model liquids, in Table 1.

As under steady flow conditions the polarization of the rear probe segment does not affect the concentration boundary layer established at the front probe segment, this front segment works in a similar way as a single probe. By contrast the rear segment is in the concentration shade of the front one and it gives the lower current signal. For the steady wall shear rate the ratio of both the measured current signals has a constant value $I_R = I_2/I_1$, which is dependent only on the relative thickness of the insulating gap g_i/l. The experimental value of $I_R = 0.663 \pm 0.007$ obtained for our probe geometry ($g_i/l \simeq 0.1$) was close to that of $I_R = 0.645$ predicted for this geometry by the theoretical analysis [22].

Both asymptotes of the transient process after polarization switch-on, obtained for $t \to 0$ (Equation 4) and for $t \gg t_0$ (Equation 3), respectively, are schematically shown in Figure 5. This Figure also demonstrates the physical meaning of the probe characteristic time t_0. For a probe of given shape, the magnitudes of both

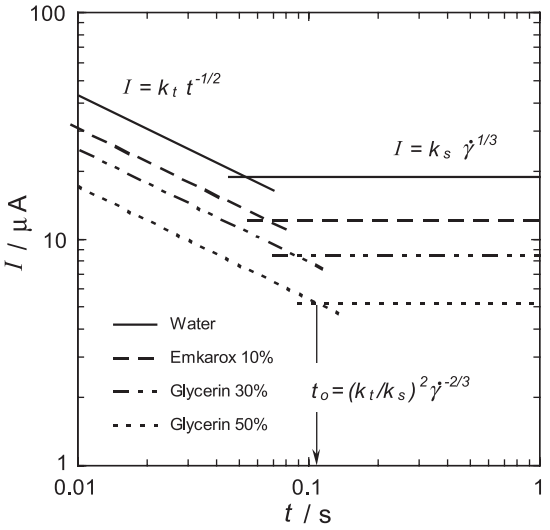

Fig. 5. Asymptotes of current responses on the probe polarization switch-on obtained for the front probe segment at $\bar{\dot{\gamma}}(t) = 100\ s^{-1}$.

calibration constants are sensitive only to the diffusivity of active ferricyanide ions in the solution. The diffusion coefficient diminution renders the probe characteristic time longer and the probe dynamic response slower. As seen in Table 1 the diffusion coefficients D_s and D_t, which were calculated from the experimental values of k_s and k_t by using Equations 5 and 6, are in good agreement for all the model solutions.

4.2. *Dynamic behaviour of the probe under fluctuating flow conditions*

The time traces of fluctuating wall shear rate measured by the two-strip probe at three different operating conditions are shown in Figure 6. The thick lines denote the correct courses of wall shear rate calculated for the film flow conditions according to Equation 11. The thin lines correspond to the quasisteady interpretation of the current signal measured by the front probe segment, $(I_1(t)/k_s)^3$. Due to the probe inertia, this quasisteady signal exhibits a certain amplitude attenuation and a phase shift in respect to the correct one. The circle symbols represent the corrected electrodiffusion data obtained by the application of the simple approximate model (Equation 2). The correction formula works well even when the amplitude of the flow fluctuations is relatively high (Figure 6(a)). Significant deviations between the actual and measured value of the wall shear rate are observed, only if flow reversal conditions are approached, $\tilde{\dot{\gamma}}/\bar{\dot{\gamma}} \simeq 1$ (Figure 6(b)). These deviations are apparent mainly in the region of low wall shear rates. The corrected signal underestimates the minimum value (about 20% in Figure 6(b)), but the signal maximum is still determined quite well. When the flow conditions corresponding to the strong flow reversal are adjusted, the electrodiffusion signal distortion is more pronounced (Figure 6(c)). However, the slightly negative minimum values of the wall shear rate provided by the approximate model serves as evidence of the flow reversal.

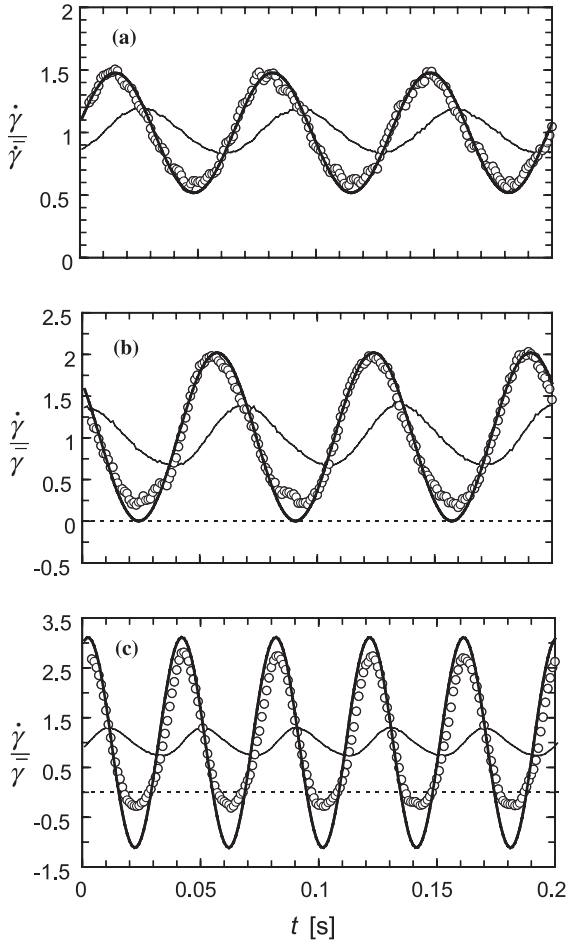

Fig. 6. Time courses of fluctuating wall shear rate measured for Emkarox 10%. Correct course of wall shear rate (Equation 11, *thick lines*), the quasisteady electrodiffusion signal (Equation 1, *thin lines*), and the corrected electrodiffusion data (Equation 2, *circles*) obtained under oscillating film flow conditions: (a) $f = 15$ Hz, $h = 0.58$ mm, $a = 0.4$ mm, $\bar{\dot{\gamma}}(t) = 175\ s^{-1}$, $\tilde{\dot{\gamma}}/\bar{\dot{\gamma}} = 0.50$, $\Omega = 3.7$; (b) $f = 15$ Hz, $h = 0.58$ mm, $a = 0.8$ mm, $\bar{\dot{\gamma}}(t) = 175\ s^{-1}$, $\tilde{\dot{\gamma}}/\bar{\dot{\gamma}} = 1.02$, $\Omega = 3.7$; (c) $f = 25$ Hz, $h = 1.09$ mm, $a = 0.6$ mm, $\bar{\dot{\gamma}}(t) = 146\ s^{-1}$, $\tilde{\dot{\gamma}}/\bar{\dot{\gamma}} = 2.17$, $\Omega = 8.3$.

The normalized current signals provided by the two-strip probe are compared in Figure 7. Due to the different dynamic behaviour of the probe segments, the measured signals differ in their amplitudes and phase shifts. Consequently, the current ratio signal, $I_R(t) = I_2/I_1$, has a fluctuating character with an amplitude which is sensitive to the magnitude of the wall shear rate fluctuations.

All data on the frequency response of the probe segments obtained under relatively small flow fluctuations (for $\tilde{\dot{\gamma}}/\bar{\dot{\gamma}} < 0.25$) are presented in Figure 8. The amplitude attenuations and the phase shifts measured for the front probe segment (solid symbols) follow the numerical predictions (solid lines) very well, whereas the same data obtained for the rear probe segment (open symbols) follow these predictions (dashed lines) only if the non-dimensional frequency of wall shear rate fluctuations is low. In this case the effect of the insulating gap, which is neglected in the numerical calculation, is

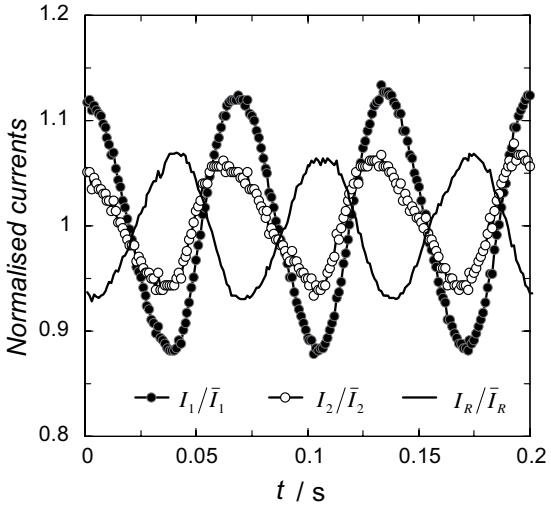

Fig. 7. Current response of the two-strip probe on the fluctuating wall shear rate (see caption under Figure 6(b) for flow conditions).

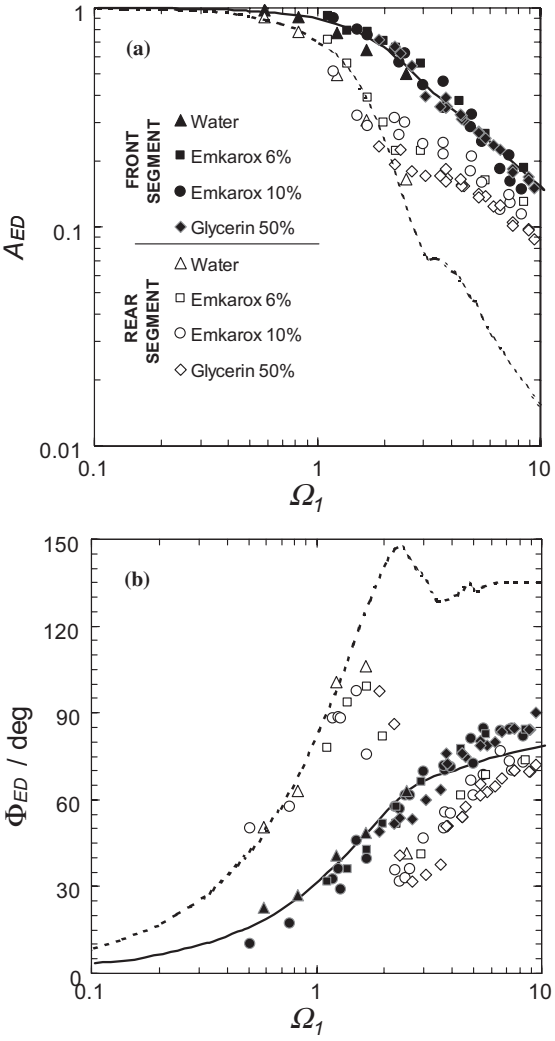

Fig. 8. Frequency response of the two-strip probe. Comparison of experimental data (*solid* and *open symbols*) with numerical prediction (*solid* and *dashed lines* for the front and rear strip, respectively).

not significant. When the non-dimensional frequency reaches the value of $\Omega_1 \simeq 1.5$, the dynamic behaviour of the rear segment suddenly changes due to a secondary edge effect, which takes place just behind the insulating gap. After reaching its maximum value of $\Phi_{ED} \sim 100°$, the phase shift of the rear segment signal falls rapidly to a local minimum of $\Phi_{ED} \sim 25°$ at $\Omega_1 \simeq 2.5$. For higher frequencies ($\Omega_1 > 2$) the rear segment signal exhibits even less significant phase shift than the front one and, under the same conditions, the amplitude attenuation measured for this signal is not so pronounced as that predicted by the numerical calculation. An additional theoretical analysis, which would include the influence of the insulating gap on the probe dynamics, is needed to explain the observed frequency response of the rear segment.

The amplitude of current ratio fluctuations was found to be proportional to the imposed amplitude of wall shear rate fluctuations. This dependence is shown in Figure 9, where measurements done at three frequencies of the fluctuating wall shear rate are compared. The relation between the relative amplitudes of the imposed input signal ($\tilde{\dot{\gamma}}/\bar{\dot{\gamma}}$) and measured output signal ($\tilde{I}_R/\bar{I}_R$) remains practically linear, even when flow reversal is reached. If the frequency of the imposed wall shear rate fluctuations is increased, the amplitude attenuation of the measured current signals becomes more pronounced and thus the slope of the lines shown in Figure 9 decreases.

After putting all the measured data together into Figure 10, it was found that the ratio of the relative amplitudes, $A_R \equiv (\tilde{I}_R/\bar{I}_R)/(\tilde{\dot{\gamma}}/\bar{\dot{\gamma}})$, is dependent only on the dimensionless frequency $\Omega_1 \equiv \omega(k_t/\bar{I}_1)^2$. The following power dependence fits all the data obtained for dimensionless frequencies $\Omega_1 > 2$

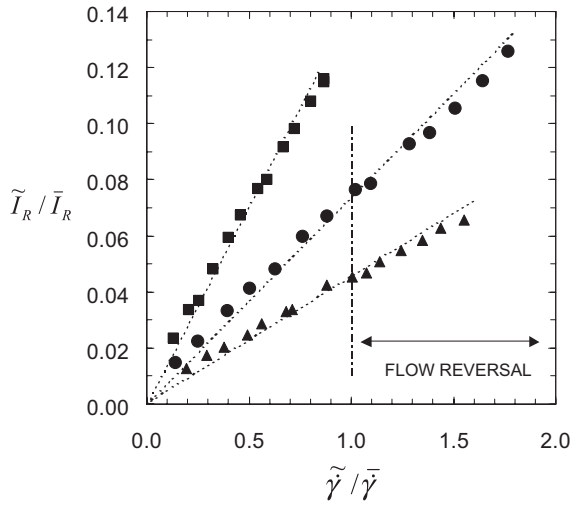

Fig. 9. Growth of relative amplitude of current ratio signal due to enhancement of wall shear rate fluctuations observed for the oscillating liquid film flow of Emkarox 10% ($h = 0.58$ mm, $\bar{\dot{\gamma}} = 175\ s^{-1}$). Parameters of oscillations: $f = 10$ Hz, $a = 0.3 \div 1.4$ mm (*squares*), $f = 15$ Hz, $a = 0.2 \div 1.4$ mm (*circles*), and $f = 20$ Hz, $a = 0.15 \div 0.8$ mm (*triangles*).

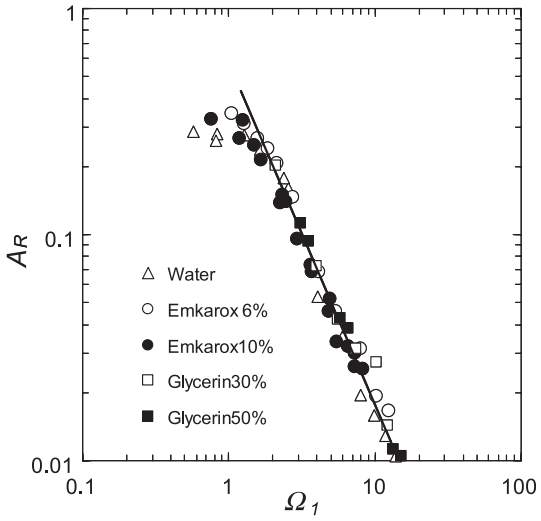

Fig. 10. Dependence of the amplitude ratio A_R on the dimensionless frequency of wall shear rate fluctuations Ω_1.

$$A_R = 0.565\,\Omega_1^{-3/2} \tag{14}$$

The simple relation $\widetilde{I}_R/\bar{I}_R > 0.565\,\Omega_1^{-3/2}$ (valid only for $\widetilde{\dot{\gamma}}/\bar{\dot{\gamma}} > 1$) can be then used as a criterion for detection of the unsteady flow reversal directly from the measured current signals. This signal processing method, which is able to detect even a short-time flow reversal, will be demonstrated in the following section.

4.3. *Wall shear rate under large solitary waves*

The typical time courses of the film thickness and the wall shear rate obtained for the solitary wave regime are shown in Figure 11. This regime of regular waves was excited by low-frequency pulsations ($f_P = 1.8$ Hz) of the inlet flow rate of water ($Q = 0.000\,091$ m^2 s^{-1} and $Re = 91$). The presented signals, which were simultaneously recorded by the capacitance and electrodiffusion probe at the downstream measurement location ($X = 1.5$ m), are normalized by their time-average values. The solitary wave crests reach a value almost two times higher than that of the mean film thickness and the peak-to-peak distance between them is long ($c/f_P = 152$ mm). The short capillary waves ($\lambda \sim 5$ mm and $f \sim 53$ Hz) are not so clearly seen on the film surface profile, because the signal from the capacitance probe underestimates their amplitudes. This is caused by the averaging effect of the cylindrical probe of diameter 3 mm. The wall shear rate profile, obtained after application of the correction formula (Equation 2) to measured electrodiffusion data, exhibits the same characteristic features as that obtained from the numerical simulation [19]. Strong fluctuations of the wall shear rate are apparent in the region of capillary waves. Then steep increasing of the wall shear rate is observed, with the maximum value located just in front of the large wave crest. Finally, gradual relaxation of the wall shear rate takes place in the wave trail region. The most interesting feature is the existence of a small backflow region characterized by negative values of the wall shear rate. The flow in front of the solitary wave is highly unsteady and this is why the observed near-wall flow reversal takes only a few microseconds.

Two possible approaches to the identification of this near-wall flow reversal from measured electrodiffusion data are presented in Figure 12, where the wall shear rate modulation in front of the large solitary wave is shown in detail. The first approach, based on the signal correction according to the approximate model of probe dynamics, is demonstrated in Figure 12(a). It is clearly seen that the signal correction in respect to the probe dynamics is really important, because rapid flow changes in the near-wall region bring about strong fluctuations of the current measured by the front probe segment. The negative values of wall shear rate, apparent after signal correction ($\dot{\gamma}_{min} = -375$ s^{-1} for data from Figure 12(a)), suggest that there is indeed a backflow region in the liquid film. As the approximate model underestimates, under reverse flow conditions, the minimum values of wall shear rate, the backflow in this small region will probably be even stronger.

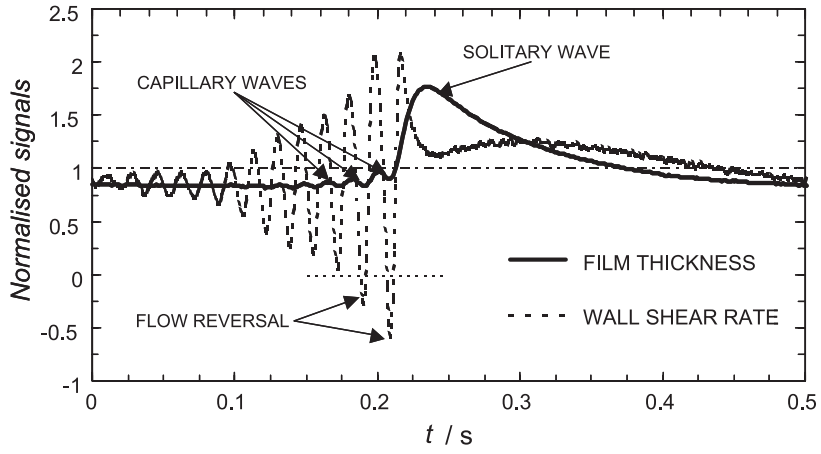

Fig. 11. Time courses of film thickness and wall shear rate typical for the solitary wave regime. Data measured for the film flow of water at $f_P = 1.8$ Hz, $Re = 91$, $\alpha = 6.5°$, $X = 1.5$ m, $c = 0.28$ m s^{-1}, $\bar{\dot{\gamma}} = 635$ s^{-1}.

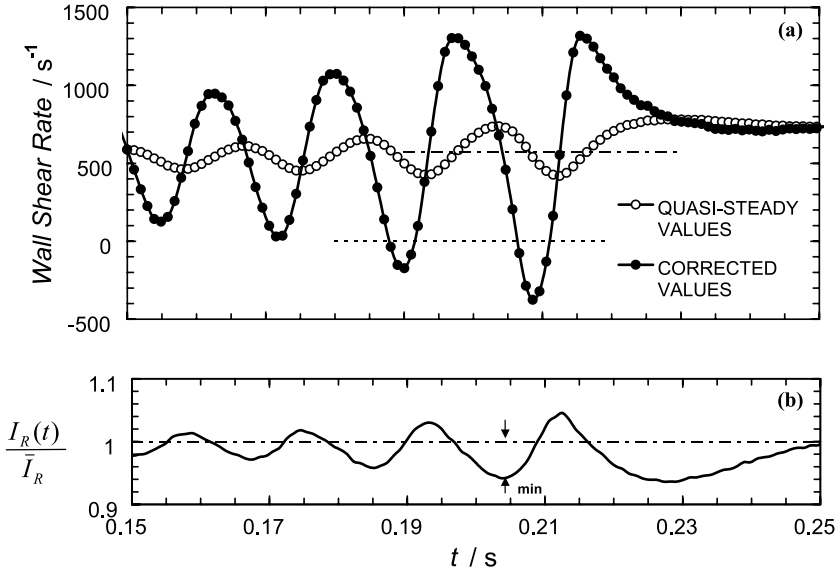

Fig. 12. Fluctuating wall shear rate in front of the large solitary wave (see caption under Figure 11 for the flow conditions). Estimation of wall shear rate minimum from (a) corrected electrodiffusion data, (b) amplitude of the current ratio signal.

The second approach to flow reversal detection, which is demonstrated in Figure 12(b), analyses the fluctuating current ratio signal. Assuming that the proportional relation between the wall shear rate and the current ratio amplitudes (Equation 14) also holds under not strictly periodic flow conditions, an estimate of the wall shear rate minimum can be obtained. First, the value of dimensionless frequency Ω_1, which characterizes the flow conditions in front of the solitary wave, has to be calculated. The value of $\Omega_1 \simeq 8$, corresponding to the frequency of the observed capillary waves ($f \simeq 53$ Hz) and to the probe characteristic time ($t_0 \simeq 24$ ms for $\bar{I}_1 \simeq 28$ μA), is obtained for the measured electrodiffusion signal. Then Equation 14 provides for the criterion of flow reversal achieving the condition $\widetilde{I}_R/\bar{I}_R > 0.025$ ($A_R = 0.025$ for the given value of $\Omega_1 = 8$). This condition is met in the present film flow experiment, because the value of $\widetilde{I}_R/\bar{I}_R \simeq 0.058$ corresponds to the current ratio minimum depicted in Figure 12(b). According to Equation 14, this amplitude of the current ratio signal is achieved at relatively high amplitudes of wall shear rate fluctuation $\widetilde{\dot{\gamma}}/\bar{\dot{\gamma}} \simeq 2.32$. Finally, considering the mean level of wall shear rate in the capillary wave region ($\bar{\dot{\gamma}} \simeq 573$ s^{-1}), the value of $\dot{\gamma}_{\min} = -755$ s^{-1} can be obtained for the wall shear rate minimum. We suppose that this more negative estimate predicts the strength of backflow in front of the measured solitary wave well.

5. Conclusion

The calibration experiments carried out under fluctuating flow conditions provided a new insight into the dynamic behaviour of two-segment electrodiffusion probes. It was found that:

(i) The theoretical frequency response function for a single wall probe can be approximated well by the simple formula (Equation 8) that follows from this similarity approximation to the corresponding mass-transfer problem.

(ii) The simple approximate model of the wall probe dynamics (Equation 2) works well even when flow fluctuations in the near-wall region are relatively large and fast, but the flow still remains without a reversal.

(iii) The amplitude of the current ratio signal measured by the two-strip probe is proportional to the magnitude of the wall shear rate fluctuations. The simple relationship (Equation 14), which was obtained for high-frequency fluctuations, is valid even under flow reversal conditions in the near-wall region.

(iv) The two-strip electrodiffusion probe is able to detect even a short-time flow reversal in the near-wall region. The wall shear rate measurements, which were done under wavy film flow conditions, confirm the existence of a small backflow region located just in front of the large solitary wave.

Acknowledgement

This work was supported by the Grant Agency of the Academy of Sciences of the Czech Republic under grant A4072914.

References

1. T. Mizushina, The electrochemical method in transport phenomena, *in* T.F. Irvine and J.P. Hartnett (Eds), 'Advances in Heat Transfer' Vol. 7 (Academic Press, 1971), p. 87.

2. T.J. Hanratty and J.A. Campbell, Measurement of wall shear stress, *in* J.R. Goldstein (Ed.), 'Fluid mechanics measurements' (Washington, Hemisphere, 1983), p. 559.
3. V.E. Nakoryakov, A.P. Burdukov, O.N. Kashinsky and P.I. Geshev, *in* V.E. Gasenko (Ed.), 'Electrodiffusion method of investigation into the local structure of turbulent flows' Novosibirsk, 1986 (in Russian).
4. C. Deslouis, O. Gil and B. Tribollet, *J. Fluid Mech.* **215** (1990) 85.
5. O. Wein, V. Sobolík and J. Tihon, *Collect. Czech. Chem. Commun.* **62** (1997) 420.
6. C. Deslouis, O. Gil and B. Tribollet, *Int. J. Heat Mass Transf.* **33** (1990) 2525.
7. P. Kaiping, *Int. J. Heat Mass Transf.* **26** (1990) 545.
8. A.A. van Steenhoven and F.J.M.H. van de Beucken, *J. Fluid Mech.* **231** (1991) 599.
9. Z.K. Mao and T.J Hanratty, *Int. J. Heat Mass Transf.* **34** (1991) 281.
10. A.N. Menendez and B.R. Ramaprian, *J. Fluid Mech.* **161** (1985) 139.
11. V. Sobolík, O. Wein and J. Čermák, *Collect. Czech. Chem. Commun.* **52** (1987) 913.
12. D.M. Wang and J.M. Tarbell, *Int. J. Heat Mass Transf.* **36** (1993) 4341.
13. J.S. Son and T.J Hanratty, *J. Fluid Mech.* **35** (1969) 353.
14. B. Py and J. Goose, *C.R. Acad. Sci.* **269A** (1969) 401.
15. D.J. Tagg, M.A. Patrick and A.A. Wragg, *Trans. Inst. Chem. Eng.* **57** (1979) 176.
16. C. Tournier and B. Py, *J. Fluid Mech.* **85** (1978) 161.
17. C. Deslouis, B. Tribollet, R. Comolet and G. Vlachos, 'La Houille Blanche' (**6** 1987), p. 459.
18. H.C. Chang, *Annu. Rev. Fluid Mech.* **26** (1994) 103.
19. N.A. Malamataris, M. Vlachogiannis and V. Bontozoglou, *Phys. Fluids* **14** (2002) 1082.
20. B. Py, *Exp. Fluids* **8** (1990) 281.
21. R.J. Bauer and C.H. von Kerczek, *J. Appl. Mech.* **58** (1991) 278.
22. O. Wein and K. Wichterle, *Collect. Czech. Chem. Commun.* **54** (1989) 3198.